Movement of Voltage Sensor S4 in Domain 4 Is Tightly Coupled to Sodium Channel Fast Inactivation and Gating Charge Immobilization

Frank J.P. Kühn and Nikolaus G. Greeff

From the Physiologisches Institut, Universität Zürich, CH-8057 Zürich, Switzerland

abstract The highly charged transmembrane segments in each of the four homologous domains (S4D1–S4D4) represent the principal voltage sensors for sodium channel gating. Hitherto, the existence of a functional specialization of the four voltage sensors with regard to the control of the different gating modes, i.e., activation, deactivation, and inactivation, is problematic, most likely due to a functional coupling between the different domains. However, recent experimental data indicate that the voltage sensor in domain 4 (S4D4) plays a unique role in sodium channel fast inactivation. The correlation of fast inactivation and the movement of the S4D4 voltage sensor in rat brain IIA sodium channels was examined by site-directed mutagenesis of the central arginine residues to histidine and by analysis of both ionic and gating currents using a high expression system in *Xenopus* oocytes and an optimized two-electrode voltage clamp. Mutation R1635H shifts the steady state inactivation to more hyperpolarizing potentials and drastically increases the recovery time constant, thereby indicating a stabilized inactivated state. In contrast, R1638H shifts the steady state inactivation to more depolarizing potentials and strongly increases the inactivation time constant, thereby suggesting a preferred open state occupancy. The double mutant R1635/1638H shows intermediate effects on inactivation. In contrast, the activation kinetics are not significantly influenced by any of the mutations. Gating current immobilization is markedly decreased in R1635H and R1635/1638H but only moderately in R1638H. The time courses of recovery from inactivation and immobilization correlate well in wild-type and mutant channels, suggesting an intimate coupling of these two processes that is maintained in the mutations. These results demonstrate that S4D4 is one of the immobilized voltage sensors during the manifestation of the inactivated state. Moreover, the presented data strongly suggest that S4D4 is involved in the control of fast inactivation.

key words: mutagenesis • voltage sensor • gating current • two-electrode voltage clamp

introduction

Voltage-gated sodium channels are highly specialized membrane proteins that react rapidly to small changes of the membrane potential (Hodgkin and Huxley, 1952). A series of experimental data indicate that the molecular voltage sensors of these proteins are represented mainly by four putative transmembrane segments known as S4 helices, which contain a highly conserved regular pattern of positively charged amino acid residues (Catterall, 1986; Noda et al., 1986; Aggarwal and MacKinnon, 1996; Seoh et al., 1996). During channel activation, the S4 segments move outward stepwise in response to a depolarization of the membrane potential (Stühmer et al., 1989; Durell and Guy, 1992; Sigworth, 1993; Yang and Horn, 1995). These voltage-dependent displacements represent a series of conformational changes inside the channel protein that finally result in the opening of the ion-selective pore. The movement of the charged voltage sensors produces a measurable electric displacement current called gating current because of its strong correlation with channel gating. The time integral of the gating current reflects the charge moved by the voltage sensors in response to changes of the membrane electric field. The analysis of gating currents provides much information about transitions between 'silent' channel states where no ionic current flows, i.e., between closed and inactivated states. During a few milliseconds of maintained depolarization, the sodium channel spontaneously closes to an inactivated state (for recent reviews see Papazian and Bezanilla, 1997; Armstrong and Hille, 1998). For squid sodium channels it was shown that inactivation immobilizes a considerable part of the gating charge by an as yet unknown mechanism and that both recovery from inactivation and recovery of immobilized charge have the same time course (Armstrong and Bezanilla, 1977). On the other hand, it was demonstrated that the voltage dependence of inactivation is closely coupled to the activation process (Aldrich et al., 1983; Catterall, 1986; Stühmer et al., 1989; Papazian et al., 1991). This coupling mechanism was discovered to be strongly disturbed by a naturally occurring mutation in S4D4 of the human skeletal muscle sodium channel (Ptàcek et al., 1992). The mutation has only minor effects on acti-

Address correspondence to Nikolaus G. Greeff, Physiologisches Institut, Universität Zürich, Winterthurerstr. 190, CH-8057 Zürich, Switzerland. Fax: 41-1-635-6814; E-mail: greeff@physiol.unizh.ch

vation but considerably changes the inactivation properties of the channel (Chahine et al., 1994). However, in potassium channels the corresponding mutation concerning all of the four identical subunits affects both activation and inactivation (Papazian et al., 1991). These findings suggest that in voltage-dependent sodium channels there is some functional specialization of the four different S4 voltage sensors with regard to the gating processes. This may correspond to the original hypothesis of Hodgkin and Huxley (1952) who proposed three *m* gates that underlie activation and an *h* gate that mediates inactivation. Meanwhile, a series of experimental data supports the hypothesis that S4D4 is particularly involved in sodium channel fast inactivation (Chahine et al., 1994; Sheets and Hanck, 1995; Yang and Horn, 1995; Yang et al., 1996; Chen et al., 1996; Kontis and Goldin, 1997; McPhee et al., 1998; Cha et al., 1999). For instance, Yang et al. (1996) have demonstrated that only two of the outermost positively charged S4 arginines (R2, R3) in domain 4 move completely from an internally accessible to an externally accessible location during depolarization and therefore are good candidates for mediating the principal voltage sensitivity of S4D4. However, the role of the equally highly conserved arginines of the central and innermost part of this segment is currently unclear.

Previously, the special role of S4D4 in sodium channel gating was analyzed mainly by measuring ionic currents at single channel or whole cell level. An additional and more direct insight into the gating machinery of these channels is obtained from gating current measurements (Conti and Stühmer, 1989; Moran and Conti, 1990; Sheets and Hanck, 1995). For instance, using a combination of site-directed fluorescent labeling and gating current recording it was recently shown that the voltage sensors in domain 3 and 4, but not 1 and 2, are immobilized during sodium channel fast inactivation (Cha et al., 1999).

By performing both gating current and ionic current studies of rat brain (rB)IIA[1] sodium channel mutants expressed in *Xenopus* oocytes we were able to give closer insights into the tight structural and functional coupling of S4D4 to the inactivation machinery of the channel. The data show that the mutation of the central arginine residues (R1635H, R1635/1638H, and R1638H) have profound and specific effects on both the inactivation and immobilization properties of the channel. These findings strongly support the hypothesis that S4D4 is the outstanding voltage sensor involved in sodium channel fast inactivation.

[1]*Abbreviations used in this paper:* cRNA, complementary RNA; E_{Na}, sodium reversal potential; $I_{g,n}$, non-immobilized gating current fraction; $I_{g,t}$, total gating current fraction; rBIIA, rat brain IIA; R_s, series resistance; TEVC, two-electrode voltage clamp; TTX, tetrodotoxin; WT, wild-type.

materials and methods

Mutagenesis and Expression of Channels

The cDNA of wild-type rBIIA sodium channel α subunit used in this study was derived from plasmid pVA2580 and transferred into high expression vector pBSTA (both plasmids kindly provided from Dr. A. Goldin, Department of Microbiology and Molecular Genetics, University of California, Irvine, CA). The resulting plasmid pBSTA(α) contains a T7 RNA polymerase promoter and *Xenopus*-β-globin 5′ and 3′ untranslated sequences that greatly increase the expression of exogenous proteins in oocytes (Shih et al., 1998). Site-directed mutagenesis was performed using the QuikChange mutagenesis system (Stratagene Corp.). The template for the PCR-based mutagenesis reaction was the 3,544-bp BglII-SacII subfragment of pBSTA(α) subcloned into vector pBSTA. The supercoiled double-stranded DNA template was annealed with two synthetic oligonucleotide primers that contained the desired mutation and were complementary to opposite strands of the vector. Primer extension was performed during temperature cycling using high fidelity Pfu DNA polymerase. Subsequently, the parental dam–methylated DNA template was destroyed by DpnI digestion and the mutation-containing synthesized DNA was transformed into *Escherichia coli* XL1-Blue supercompetent cells (Stratagene Corp.). Mutagenic oligonucleotides were designed such that restriction endonuclease recognition sites were created or deleted. Thus, the desired mutations could be identified by restriction endonuclease analysis of the recombinant plasmid clones. In addition, every mutation was verified by DNA sequencing. Finally, the mutated BglII-SacII subfragment was transferred back into pBSTA(α). At least two independent clones of each mutant were tested to exclude effects of inadvertent mutations in other regions of the channel. Capped, full-length transcripts were generated from SacII linearized plasmid DNA using T7 RNA polymerase (mMessage mMachine In vitro Transcription Kit; Ambion Inc.). Oocytes (stage V–VI) from *Xenopus laevis* (NASCO) were used. 1 d before injection of complementary RNA (cRNA), the oocytes were defolliculated in a Ca^{2+}-free solution containing 2 mg/ml collagenase (Boehringer Mannheim) for ~1 h at room temperature. Oocytes were microinjected with 20–40 ng of cRNA (50 nl) and maintained at 18 ± 1°C in Modified Barth's Solution (88 mM NaCl, 2.4 mM $NaHCO_3$, 1 mM KCl, 0.82 mM $MgSO_4$, 0.41 mM $CaCl_2$, 0.33 mM $Ca(NO_3)_2$, 10 mM Hepes-CsOH, pH 7.5, supplemented with 25 U penicillin, 25 μg/ml streptomycin-sulfate, and 50 μg/ml gentamycin-sulfate. For the recording of gating currents, 2 μM tetrodotoxin (TTX; RBI-Research Biochemicals International) was added.

Electrophysiology and Data Acquisition

Two-electrode voltage clamp (TEVC) recordings were performed 1–8 d after cRNA injection with a TEC-05 (npi-electronic) that had been modified for optimized compensation of the series resistance (R_s) and for fast charging of the membrane capacitance (Greeff and Polder, 1998). Intracellular agarose cushion electrodes (Schreibmayer et al., 1994) were filled with 3 M KCl and had a resistance between 100 and 300 kΩ. Macroscopic ionic and gating current signals were recorded using a PDP-11/73 computer (Digital Equipment Corp.) controlling a 16-bit A/D and 12-bit D/A interface (CED). The oocytes were clamped at a holding potential of −100 mV for at least 5 min to ensure recovery from slow inactivation before recording started. The experiments were done at a temperature of +15 ± 1°C controlled by a Peltier element, unless otherwise stated. R_s compensation was adjusted to accelerate the settling time of capacitance transients within 200 μs (without low pass filtering, see below). No ana-

logue subtraction was used, since the 16-bit ADC had a sufficiently fine resolution for digital subtraction of the linear transient and leak currents by scaled averages from pulses between −120 and −150 mV. Reduction of the remaining asymmetry was achieved by finding a compromise between clamping speed and asymmetry, i.e., low-pass filtering the command signal at 5 kHz (eight-pole Bessel). Signals were low-pass filtered at 5 kHz (−3 dB) and sampled at 10 or 20 kHz. The actual clamp speed at the oocyte membrane was determined from the integrated capacitance transient to have a time constant between 150 and 200 μs. A small nonlinearity in leak subtraction appearing occasionally was compensated by baseline correction. Data analysis was performed on the PDP-11 and additionally with the Windows-compatible programs UN-SCAN-IT™ (Silk Scientific Corp.) and PRISM™ (GraphPad Software, Inc.).

results

Ionic Current Properties of Wild-Type and Mutant Sodium Channels

Na^+ currents obtained from *Xenopus* oocytes injected with either wild-type (WT) or mutant (R1635H; R1635/1638H; R1638H; subsequently named by the position in the S4 segment R4H; R4/5H; R5H) rBIIA sodium channel cRNA display characteristic patterns of voltage-dependent activation and inactivation (Fig. 1 A). For well-resolved gating current recordings in *Xenopus* oocytes, a very high expression of rBIIA sodium channels was necessary. For this purpose the genes of both WT and mutant sodium channels were expressed by use of a high expression vector (see Materials and Methods). Sodium peak currents of 10–40 μA, elicited between −10 and −20 mV in 88 mM external sodium, were obtained 2–4 d after injection of the corresponding cRNA. During this period, only ionic current measurements were performed, because the corresponding gating currents were still too small (<0.5 μA). R_s errors were <5 mV unless the currents exceeded ~20–30 μA, because an optimized TEVC was used (see Materials and Methods). Between days 5 and 8, gating currents increased to peaks of 3–10 μA, whereas ionic currents started to decline after reaching maximum levels of up to −100 μA (Greeff et al., 1998). For recording of pure gating current traces, the corresponding ionic currents were suppressed by application of 2 μM TTX. An example for a simultaneous recording of ionic and gating current is given in Fig. 1 A (indicated by arrows). R4/5H shows an outward gating current of ~2 μA near the sodium reversal potential (E_{Na}). This gating current is merged with the outward ionic current at more depolarizing potentials. In some special experiments, performed without the application of TTX, gating currents were recorded at E_{Na} essentially not disturbed by ionic currents (see Fig. 7 B).

Compared with WT channels, the time course of inactivation is markedly slowed in R5H and R4/5H but moderately in R4H channels. In contrast, the activation kinetics appear rather similar. The biphasic current decay most clearly visible in WT channels (Fig. 1 A) indicates a mixture of fast and slow gating channels in the oocyte membrane. This phenomenon is typical for rBIIA expression in *Xenopus* oocytes if coexpression of the β1 subunit is omitted (Patton et al., 1994), but is less distinct at high expression levels (Krafte et al., 1990). The mutant channels generally display slowed inactivation kinetics compared with WT channels and therefore a transition to a more monophasic current decay is detected. We decided to express only the α subunit because of two reasons: first, at the desired high expression levels, a negative effect of β1 coexpression on the durability of the oocytes was observed; second, we could not exclude different effects of the β1 subunit on the inactivation properties of WT and S4D4 mutant channels.

The normalized current–voltage plots of WT and mutant channels superimpose rather well (Fig. 1 B). Nevertheless, the interpretation is difficult as the inactivation kinetics of the analyzed channels are different. Besides of possible R_s effects, wild-type and mutant channels presumably have different inactivation time constant (τ_h) to activation time constant (τ_m) ratios. This might result in different peak open probabilities and therefore would distort the current–voltage curve unless τ_h and τ_m change in parallel.

The kinetics of macroscopic sodium currents were analyzed by performing single or double exponential fits from normalized current traces at −20, −5, and 20 mV in order to determine the corresponding τ_h and τ_m values (Fig. 2). WT sodium current inactivation was well fit only by a double exponential because of the coexistence of slow and fast gating channels, as already mentioned. In contrast, the mutant sodium currents were well fit by a single exponential. The speed of our TEVC was fast enough to detect an acceleration of the activation kinetics for more depolarizing potentials (Fig. 2 B). The τ_m values of WT and mutant channels do not differ significantly, but the τ_h values are profoundly increased in the mutant channels according to the sequential order: WT ($\tau_{h\ (fast)}$) < R4H < R4/5H < R5H ≅ WT ($\tau_{h\ (slow)}$). Thus, the S4D4 mutants display a strong effect on inactivation rather than on activation kinetics. The unequal effects of S4D4 mutants on the gating properties of sodium channels were also observed by other groups (Chahine et al., 1994; Chen et al., 1996; Kontis et al., 1997). Between −20 mV and 20 mV, WT and mutant channels show a more pronounced voltage dependence of activation compared with inactivation represented by the slopes in Fig. 2 B; the voltage dependencies of activation and inactivation are similar in WT and mutant channels, respectively.

WT and mutant channels display different effects on steady-state inactivation (Fig. 1 C). Compared with WT

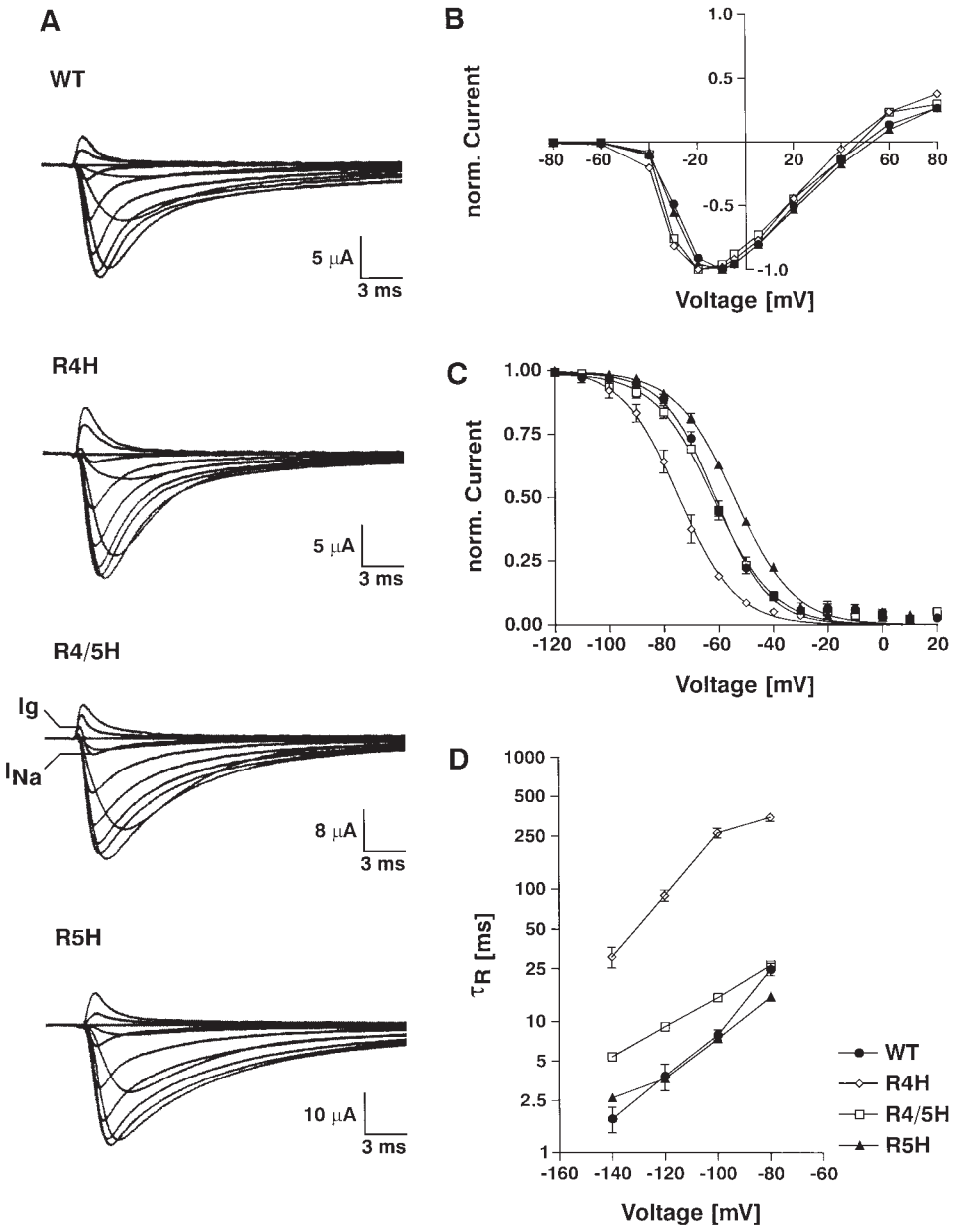

Figure 1. Effects of S4D4 point mutations on macroscopic Na^+ currents. (A) Na^+ currents from WT-, R4H-, R4/5H-, and R5H-injected *Xenopus* oocytes elicited by step depolarizations from −80 to 80 mV, holding potential −100 mV. A single trace displaying an outward gating current followed by an inward ionic current near sodium reversal potential is indicated in R4/5H. (B) Corresponding current–voltage relationship of peak Na^+ currents, normalized to the largest inward current. (C) Steady-state inactivation at 0 mV induced by a 100-ms prepulse at voltages between −120 and 20 mV, increments of 10 mV, holding potential −100 mV. The curves are fitted to a standard Boltzmann distribution with slopes and $V_{0.5}$ given in the text. Values are mean ± SEM of $n > 3$ cells. (D) Semilogarithmic plot of time constant and voltage of recovery from fast inactivation. Pulse protocol: a 80-ms test pulse to 0 mV was preceded by a 100-ms pulse to 0 mV and variable recovery periods at four different holding potentials (−80, −100, −120, and −140 mV). Values are mean recovery time constants in milliseconds ± SEM of n = 1–7 cells; WT, 1.8 ± 0.6 (−140 mV), 3.9 ± 1.8 (−120 mV), 7.9 ± 1.5 (−100 mV), 24.8 ± 6.0 (−80 mV); R4H, 30.8 ± 9.6 (−140 mV), 89.4 ± 19.3 (−120 mV), 264 ± 59 (−100 mV), 347 ± 55.1 (−80 mV); R4/5H, 5.4 ± 0.5 (−140 mV), 9.1 ± 0.9 (−120 mV), 15.1 ± 0.8 (−100 mV), 26.7 ± 1.8 (−80 mV); R5H, 2.6 (−140mV), 3.7 ± 0.2 (−120 mV), 7.4 ± 0.6 (−100 mV), 15.4 ± 0.9 (−80 mV).

(−61.1 ± 1.2 mV), the midpoint of steady-state inactivation is shifted to more hyperpolarizing potentials in R4H (−74.7 ± 1.2 mV) and shifted to more depolarizing potentials in R5H (−54.2 ± 0.9 mV). No significant shift occurs in the double mutant R4/5H (−61.8 ± 1.4 mV). The slopes of the steady-state inactivation curves, and thus the voltage dependencies, do not differ significantly: WT, 9.55 ± 1.0 mV; R4H, 10.4 ± 1.6 mV; R4/5H, 10.8 ± 1.1 mV; R5H, 10.8 ± 0.7 mV. The steady-state inactivation of R4H indicates that at more depolarizing potentials a substantial portion of the channels is maintained in the inactivated state. Therefore, R4H and R5H show opposite preferences (for the inactivated state and the open state, respectively).

The impact of the mutations on the rate of recovery from fast inactivation was tested at potentials from −80 to −140 mV. Recovery is drastically slowed in R4H, whereas R5H recovers at a speed similar to that of the WT channel (Fig. 1 D). These findings agree well with the data of Abbruzzese et al. (1998), who have demonstrated that the mutations R1449Q and R1452Q in rat skeletal muscle sodium channel (corresponding to R4 and R5 in S4D4, respectively) display opposite effects on the stability of the inactivated state. Moreover, we

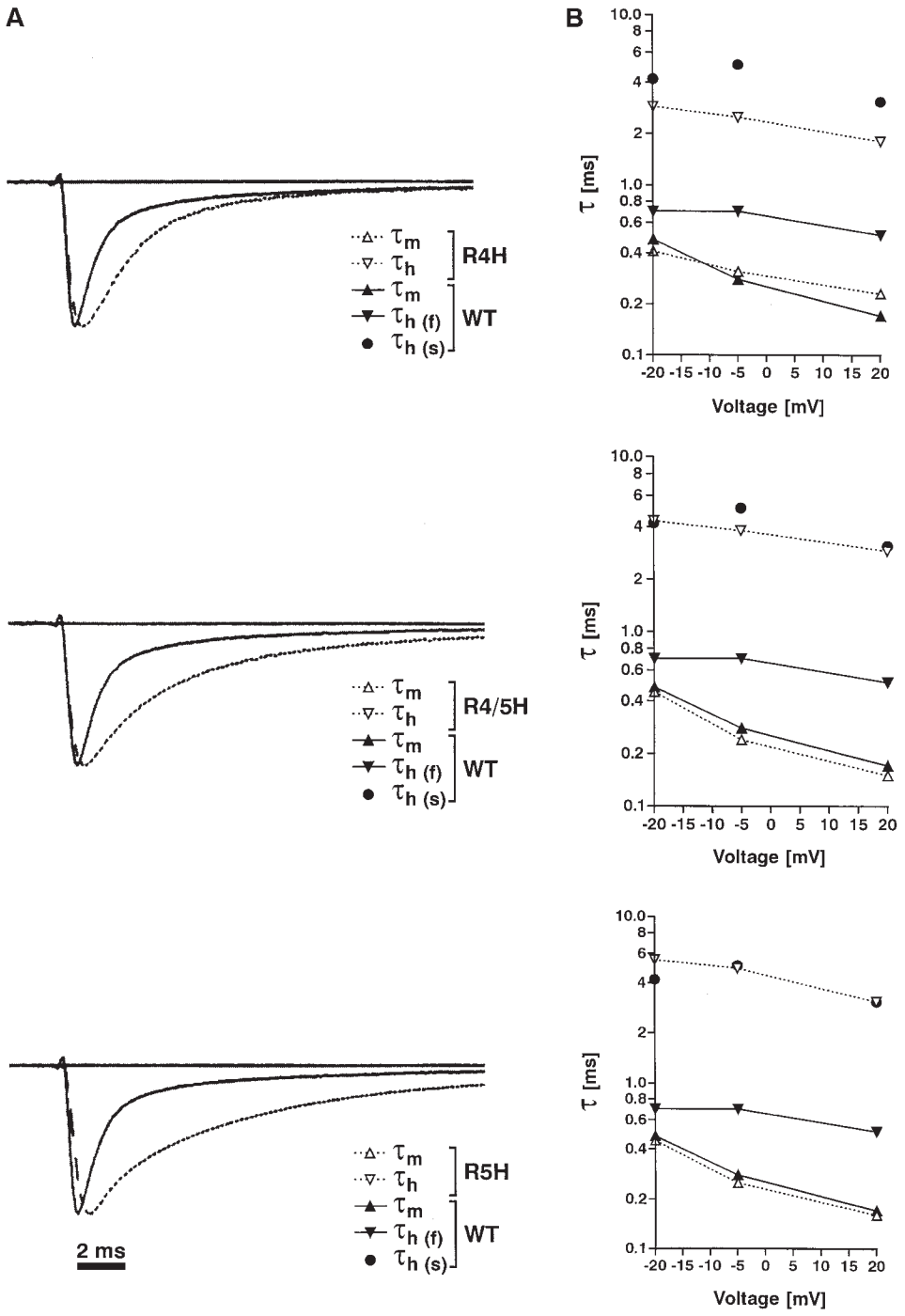

Figure 2. Effects of S4D4 point mutations on kinetics and on voltage dependence of macroscopic Na^+ currents. (A) Comparison of normalized single current traces of WT (solid line) and mutant (dotted line) channels, elicited by a depolarizing pulse to −5 mV from a −100-mV holding potential. The settling times of the corresponding capacitance transients are almost identical (data not shown). (B) Semilogarithmic plots of single (mutants) or double (WT inactivation) exponential fits, as indicated, from representative current traces elicited by depolarizing pulses to −20, −5, and 20 mV; holding potential −100 mV. Single fits accord to the following equation. $I_{Na}(t) = A * (1 - \exp(-t/\tau_m))^3 * \exp(-t/\tau_h) + P * (1 - \exp(-t/\tau_m))^3$. WT: ($\tau_m/\tau_{h\,(fast)}/\tau_{h\,(slow)}$ in ms) 0.48/0.70/4.20 (−20 mV); 0.28/0.70/5.10 (−5 mV); 0.17/0.51/3.10 (20 mV); R4H: (τ_m/τ_h in ms) 0.41/2.90 (−20 mV); 0.31/2.50 (−5 mV); 0.23/1.80 (20 mV); R4/5H: (τ_m/τ_h in ms) 0.45/4.30 (−20 mV); 0.24/3.80 (−5 mV); 0.15/2.90 (20 mV); R5H: (τ_m/τ_h in ms) 0.45/5.50 (−20 mV); 0.25/4.90 (−5 mV); 0.16/3.10 (20 mV).

found that potentials of −120 to −140 mV are necessary for total recovery, i.e., the transfer of the majority of the R4H channels from the inactivated state into the resting state. This observation is also reflected by the left-shift of the corresponding steady-state inactivation curve (Fig. 1 C). The recovery time constant of the double mutant R4/5H is increased compared with WT but to a much lesser extent than in R4H. The distinct voltage dependencies of recovery from fast inactivation in WT and mutant channels (slopes in Fig. 1 D) are similar over the total voltage range analyzed.

The results obtained from Figs. 1 and 2 clearly demonstrate an antagonism between R4H, which predominantly stabilizes the inactivated state by increasing the recovery time constant (τ_R), and R5H, which mainly impedes the entry into the inactivated state by increasing the inactivation time constant (τ_h). The inactivation properties of the double mutant are in between

the extreme positions of the single mutants with τ_h values quite similar to R5H and τ_R values also increased as in R4H, albeit to a much lesser extent.

Gating Current Properties of Wild-type and Mutant Channels

To gain further insights into the coupling of the S4D4 voltage sensor to the inactivation structure of the channel, we analyzed gating currents at the whole oocyte membrane either simultaneously with ionic currents in the same cell or in separate experiments. Compared with the cut-open oocyte method (Bezanilla et al., 1994; Stefani et al., 1994) or the macropatch technique (Conti and Stühmer, 1989), the clamp speed of standard TEVCs is regarded as considerably slower. Therefore, the TEVC seemed to be unsuitable for characterizing the kinetics of fast mode sodium channels (Ruben et al., 1997). However, we succeeded in recording well-resolved sodium channel ionic and gating currents with an optimized TEVC by finding a compromise between maximum clamping speed and minimal signal distortion (see Material and Methods). Fig. 3 D shows representative ON-gating current traces of WT and mutant channels. A significant contamination of the gating current measurements with ionic current was excluded by recording in bath solution containing 2 μM TTX. Baseline distortions, e.g., visible in the R5H record, were due to small nonlinearities in leak subtraction that occur sporadically. Before integration of gating current traces, these artifacts were minimized by baseline correction. As the ON-gating current mainly represents the sum of the charge displacements of the S4 voltage sensors during activation, the similarity of the records supports the conclusion from our ionic current studies that the activation kinetics were not significantly disturbed by the mutations. In contrast, the association of a gating current component exclusively with the inactivation process is difficult and was not specifically analyzed in this study, but there exist some positive evidence (Greeff and Forster, 1991; Sheets and Hanck, 1995).

In sodium channels the inactivation process is closely coupled to the partial gating charge immobilization, which was demonstrated by the fact that both recover with the same time course (Armstrong and Bezanilla, 1977). We used these characteristic immobilization properties to differentiate between gating currents and asymmetry artifacts that may result from incomplete subtraction of capacitance transients (Fig. 3, A–C). For this purpose, a two-pulse protocol was used; the test pulse was preceded by a conditioning pulse that prevented channel activation (Fig. 3 A). However, in the brief recovery period of 1 ms at −100 mV, the transitions between different inactivated states still produce the nonimmobilized fraction of the total gating current, which is between 50 and 60% in WT (Fig. 3 C). This observation is in accordance with the data from squid sodium channels (Armstrong and Bezanilla, 1977). The asymmetry artifact was not affected by the prepulse and therefore remained unchanged, whereas sodium ionic current essentially was inactivated (Fig. 3, B and C). These properties were also confirmed by recordings from control oocytes without sodium channel expression (data not shown).

A summary of charge–voltage plots of WT and mutant sodium channels, generated in the presence or absence of an inactivating pulse and fitted to a standard Boltzmann distribution with slopes, half-activation potentials, and degrees of gating charge immobilization, is given in Fig. 4 and Table I. R5H shows similar gating charge immobilization (48%) compared with WT (56%), whereas both R4H (34%) and R4/5H (34%) display strongly reduced gating charge immobilization. For R4H this observation reflects the fact that at more depolarizing potentials a substantial portion of the channels persists in the inactivated state (see discussion), as also indicated by the left-shift of the steady-state inactivation curve (Fig. 1 C). The slopes and half-activation potentials of WT and R5H only differ slightly from the corresponding values of R4H and R4/5H (Table I), which indicates the similar activation behavior of WT and mutant channels. The larger values of the immobilized gating charges at potentials more negative than −30 mV compared with the nonimmobilized total ON charges (Fig. 4) are most probably due to one of two possibilities. The first possibility is a contamination of the small total ON charges below −30 mV with residual ionic current in absence of an inactivating prepulse. This contamination could not be avoided at the very high expression levels and bath temperatures of 15°C despite of the presence of 2 μM TTX in the bath solution. The second possibility is an integration artifact resulting from a common baseline adjustment for the integration of gating current traces with different kinetics. However, our results were not distorted for that reason because the voltage ranges of main interest were not significantly affected.

The observed strong effects of R4H and R4/5H on gating charge immobilization clearly support the findings of Cha et al. (1999) that S4D4 is one of the voltage sensors that immobilize during sodium channel fast inactivation.

Recovery from Fast Inactivation: Correlation of Ionic and Gating Current Studies

The comparison of the recovery time courses of ionic and gating currents yields additional information about the kinetics and voltage dependence of fast inactivation in WT and mutant channels. Fig. 5 A illustrates recordings of WT ionic and gating current recoveries obtained from separate oocytes at different stages of ex-

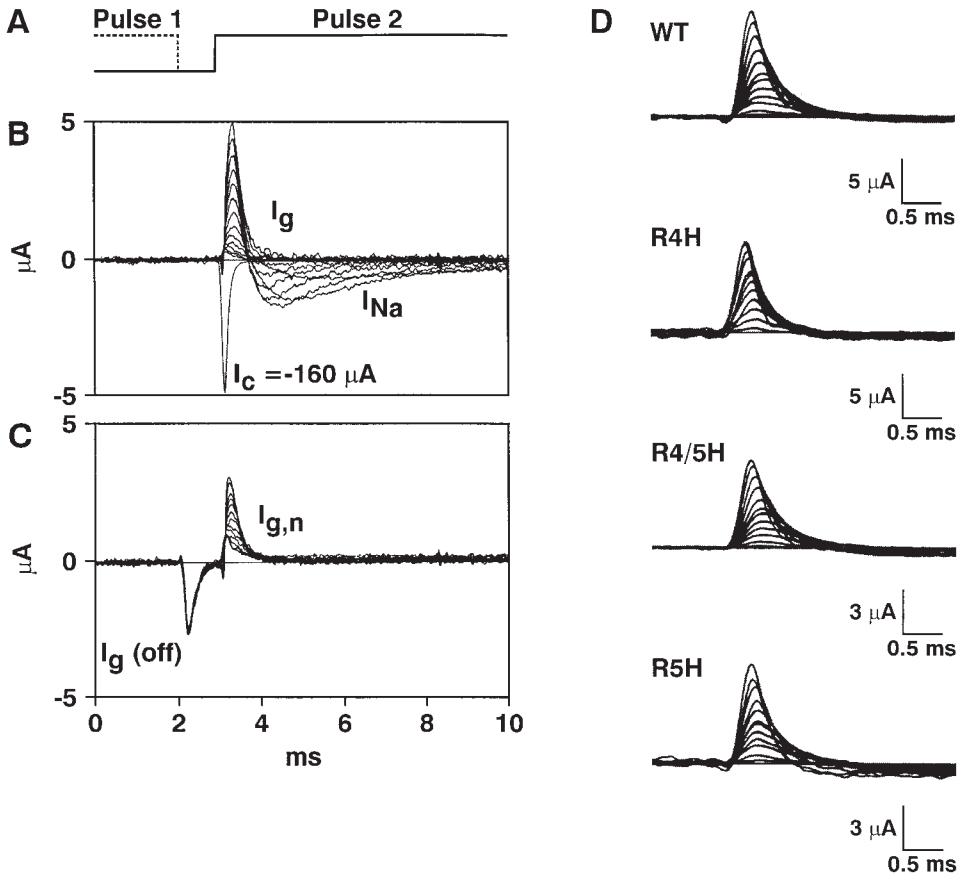

Figure 3. Gating current recordings in WT and mutant sodium channels. (A–D) Sodium ionic (I_{Na}) and gating (I_g) currents recorded from the whole cell membrane of *Xenopus* oocytes using a TEVC after blocking most (B and C) or all (D) of the ionic current with TTX. (A) Pulse protocol; the traces were elicited by 13 ms depolarizing test pulses to membrane potentials of −60 to 60 mV increasing in steps of 10 mV without (B) or with (C) a 20-ms prepulse to 0 mV from a holding potential of −100 mV, interval 1 ms at −100 mV, temperature 15°C. The OFF-gating current of the prepulse and the non-immobilized fraction of the test pulse ON-gating current ($I_{g,n}$) are indicated in C. Notice the elimination of I_{Na} and the partial immobilization (∼50%) of total gating current (I_g) due to the inactivating pulse. The corresponding capacitance current (I_c) reflects the actual clamp speed. (D) Total ON-gating currents of WT and mutant channels activated by step depolarizations in 20-mV increments from −80 to 80 mV from a holding potential of −100 mV, recorded in presence of 2 μM TTX, pulse duration 13 ms.

pression. We used an alternating pulse protocol with and without prepulse for each recovery time in order to be able to normalize for the slow peak–current decay of the reference traces (without prepulse). This current decay results from the presence of a subpopulation of slow gating channels that predominantly appear in the absence of β1 coexpression (as discussed in the context of Fig. 1). During recovery, the fast gating channels recover first, followed by the slow gating channels. The gating currents that were recorded in the presence of 2 μM TTX show a more stable reference current compared with the ionic current, thus suggesting little decay. In view of the large differences of the recovery rates of WT and R4H obtained from ionic current data (see Fig. 1 D), we decided that it was more important to analyze the close correlation of ionic and gating current recovery concerning the time course and its voltage dependence, rather than attempting to discriminate the overlapping fast and slow gating channels. The gating current recovery shows a characteristic pattern:

TABLE I

Boltzmann Parameters of Q/V Distributions in WT and Mutant Sodium Channels

Phenotype	*n*	$Q_{(t)}$-slope	$V_{(t)1/2}$	Immobilization	$Q_{(n)}$-Slope	$V_{(n)1/2}$
		mV	*mV*	*%*	*mV*	*mV*
WT	7	14.41 ± 2.27	−22.17 ± 2.23	55.57 ± 4.12	12.64 ± 1.48	−43.08 ± 2.77
R4H	5	10.36 ± 1.65	−27.80 ± 5.01	34.00 ± 4.47	12.03 ± 1.43	−43.21 ± 5.57
R4/5H	3	15.96 ± 5.95	−32.24 ± 1.69	34.33 ± 2.31	14.32 ± 3.50	−48.37 ± 3.54
R5H	4	14.99 ± 2.59	−22.62 ± 3.11	48.25 ± 4.99	12.09 ± 1.41	−41.86 ± 6.69

The data were obtained as described in Fig. 4 and fitted to a Boltzmann distribution of the form: $Y = P + (A - P)/\{1 + \exp[(V_{1/2} - V)/S]\}$. The indicated degree of immobilization represents the difference between the maximum plateaus ($A - P = Q_{max}$) of the fitted Q/V-distributions in absence (100%) and presence of an inactivating pulse. Slopes and half activation potentials of the Q/V distributions (Mean ± SD) are determined in presence ($Q_{(t)}$; $V_{(t)1/2}$) or absence ($Q_{(n)}$; $V_{(n)1/2}$) of an inactivating pulse.

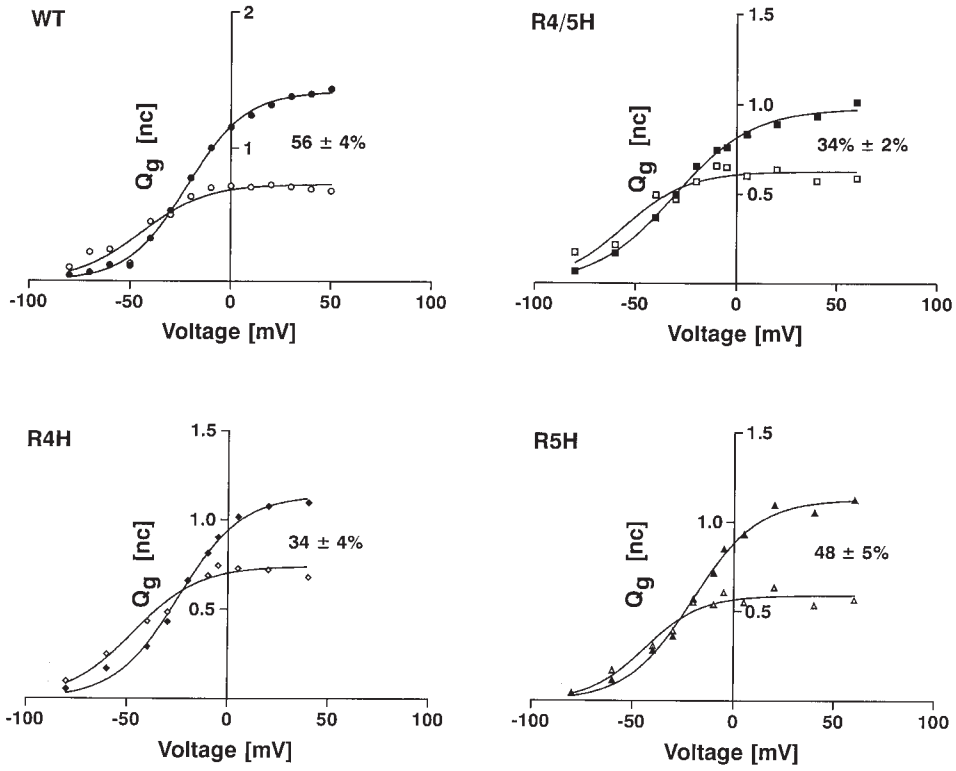

Figure 4. Charge–voltage (Q/V) distributions in WT and mutant sodium channels. Open symbols are data obtained in the presence of a 20-ms inactivating prepulse to 0 mV (1-ms interval at −100 mV). Filled symbols are data without prepulse; test pulses were 13 ms long. The gating charge (Q_g) represents the time integral of the corresponding gating current. The individual Q/V curves were fitted by a Boltzmann distribution as described in Table I. The degree of immobilization at Q_{max} derived as mean value ± SD from Table I is indicated in each diagram.

(a) the basic level where recovery starts is determined by the degree of immobilization that occurs when the duration and potential of the prepulse fully inactivate ionic current (Armstrong and Bezanilla, 1977), and (b) the recovery of the gating current in its early time course shows a discontinuous change from a rapid rise to a slower one (Greeff, 1986). We found that in WT and mutant channels ionic current and gating current recovery strongly correlate in the voltage range from −140 to −80 mV, concerning time course and voltage dependence (compare Fig. 1 D with Figs. 5–7). However, within a single phenotype the time constants of gating current recovery are significantly increased compared with the time constants of ionic current recovery. Similar results were obtained from studies of *Shaker* potassium channels where, notably at more depolarizing potentials, gating current recovery is considerably slower than is ionic current recovery (Roux et al., 1998). The observed mismatch in the corresponding recovery time constants of ionic and gating currents were obtained from data fitted with single exponential curves. Taking into account the expression of a mixture of fast and slow gating channels (Figs. 1 A and 5), we tried to fit double exponential curves, which, in some cases made the recovery time constants agree better. Nevertheless, we decided to fit our recovery data uniformly with single exponential curves since the gating charge recovery was difficult to fit by double exponential curves for two reasons: (a) the amplitude of the gating current recovery is rather small, and (b) the scattering of the data points obtained from gating charge recovery (Fig. 6 B) is more pronounced if compared with the ionic current recovery (Fig. 6 A).

Representative gating current recoveries of WT and mutant channels are given in Fig. 5 B. The reduced degree of immobilization in R4H and R4/5H compared with WT as already shown in Fig. 4 and Table I is reflected here by the increased level of the nonimmobilized gating current fraction ($I_{g,n}$) at the onset of recovery. On the other hand, the similar levels of $I_{g,n}$ in R5H and WT indicate that the degree of immobilization is not considerably altered in the mutant. A comparison of the recovery of ionic and gating current at different recovery potentials is illustrated in Fig. 6. Three different recovery potentials (−80, −100, and −120 mV) were tested in one cell, with and without an inactivating pulse, and normalized to account for current decay as described in Fig. 5. The ionic currents of both WT and mutant channels show a clear voltage dependence of recovery. At −120 mV the recovery potential is strong enough to elicit most of the slow gating channels (Fig. 6 A). The normalized gating charge recovery starts at a degree of immobilization of ~0.4 in WT and R5H at all recovery potentials, whereas R4H and R4/5H start at ~0.6 and thus show smaller fractions that recover (Fig. 6 B). This reflects the different immobilization properties of the channels, which is consistent with the data of Figs. 4 and 5. In view of the preferred occupancy of the

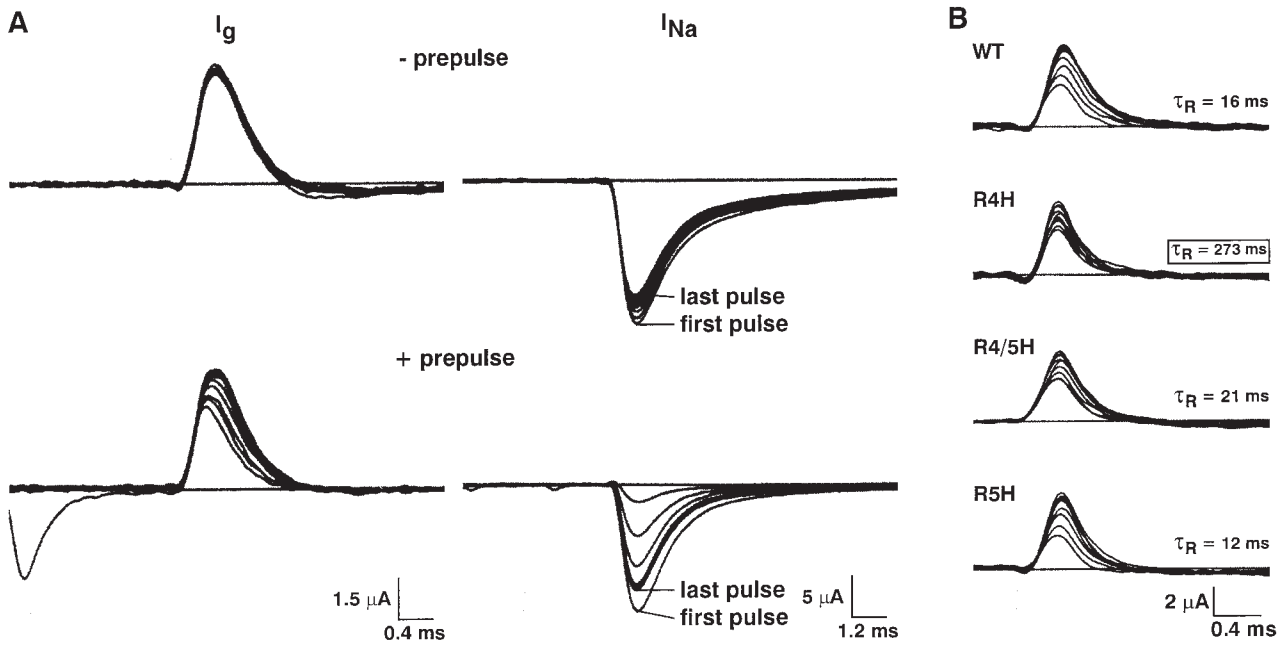

Figure 5. Recovery from fast inactivation of macroscopic ionic and gating currents. (A) Recovery of WT gating current (I_g, in the presence of 2 μM TTX) and ionic current (I_{Na}, in the absence of TTX) obtained from different oocytes. Pulse protocol: a 100-ms prepulse to 0 mV from a holding potential of −100 mV was followed by a recovery period of variable duration (2–90 ms) at −100 mV. Test pulses have a duration of 80 ms (ionic current) or 13 ms (gating current) and responses are superimposed for all recovery periods. For the calculation of the recovery time course, the current traces with prepulse were routinely normalized to the current traces without prepulse in order to compensate the slight decrease of the current amplitude during pulse series. The series of increasing recovery times, starting from 2 ms, where I_{Na} is almost totally inactivated, was preceded by the longest recovery time where the plateau of recovery is observed (first and last pulses are indicated in I_{Na} recordings). (B) Gating current recovery of WT and mutant sodium channels at −100 mV. Pulse protocol was as described above. The time intervals for recovery were between 10 and 1,250 ms for R4H and between 2 and 90 ms for WT and the other mutant channels. The recovering gating charges were fitted to a single exponential with corresponding recovery time constants (τ_R) as indicated. Notice the different levels of the nonimmobilized gating current fraction at the onset of recovery, reflecting the different degrees of immobilization.

inactivated state by R4H during more depolarizing potentials (see Fig. 1 C), one should expect that the starting point of gating current recovery in R4H depends strictly on the effective recovery potential. Indeed, the fraction of immobilized channels that recover increases for more hyperpolarizing potentials (Fig. 6 B). As observed for the ionic current, a recovery potential of −120 mV is necessary to activate the majority of the channels, and therefore the degree of immobilization in R4H gets closer to the WT level.

One of our main findings is that the time constants of gating current recovery in R4H are drastically slowed down compared with WT and parallel the recovery of the corresponding ionic current (Fig. 7 A). This observation is also true if we fit double exponential curves (data not shown). In particular, the effects of the mutations are equally pronounced in both time constants. Correspondingly, the mutations cause no shift in the relative proportions of different kinetic components. Both ionic and gating current recoveries in WT and R4H channels display a similar voltage dependence for most of the voltage range analyzed. However, at −80 mV there is obviously no correlation between the voltage dependence of ionic and gating current recovery in R4H. This apparent mismatch is due to the fact that at more depolarizing potentials a majority of the channels stay immobilized. As can be clearly derived from Fig. 6 B, the starting point of the gating charge recovery in R4H strongly depends on the effective holding potential. Consequently, at more depolarizing potentials only a minor portion of the channels participates in recovery from immobilization, yielding recovery curves with low amplitude that are difficult to fit. The strong correlation of ionic and gating current recovery concerning time course and voltage dependence was also observed in R5H and in the double mutant (data not shown).

With respect to the observation that the I_g recovery is considerably slower than the I_{Na} recovery in both WT and mutant channels we theorized that this could be due to the fact that the corresponding recoveries were accomplished in separate oocytes at different stages of expression. Consequently, we performed some recovery experiments immediately one after the other in the same cell at 8°C in order to enhance the durability of the oocytes and measured gating current recovery at

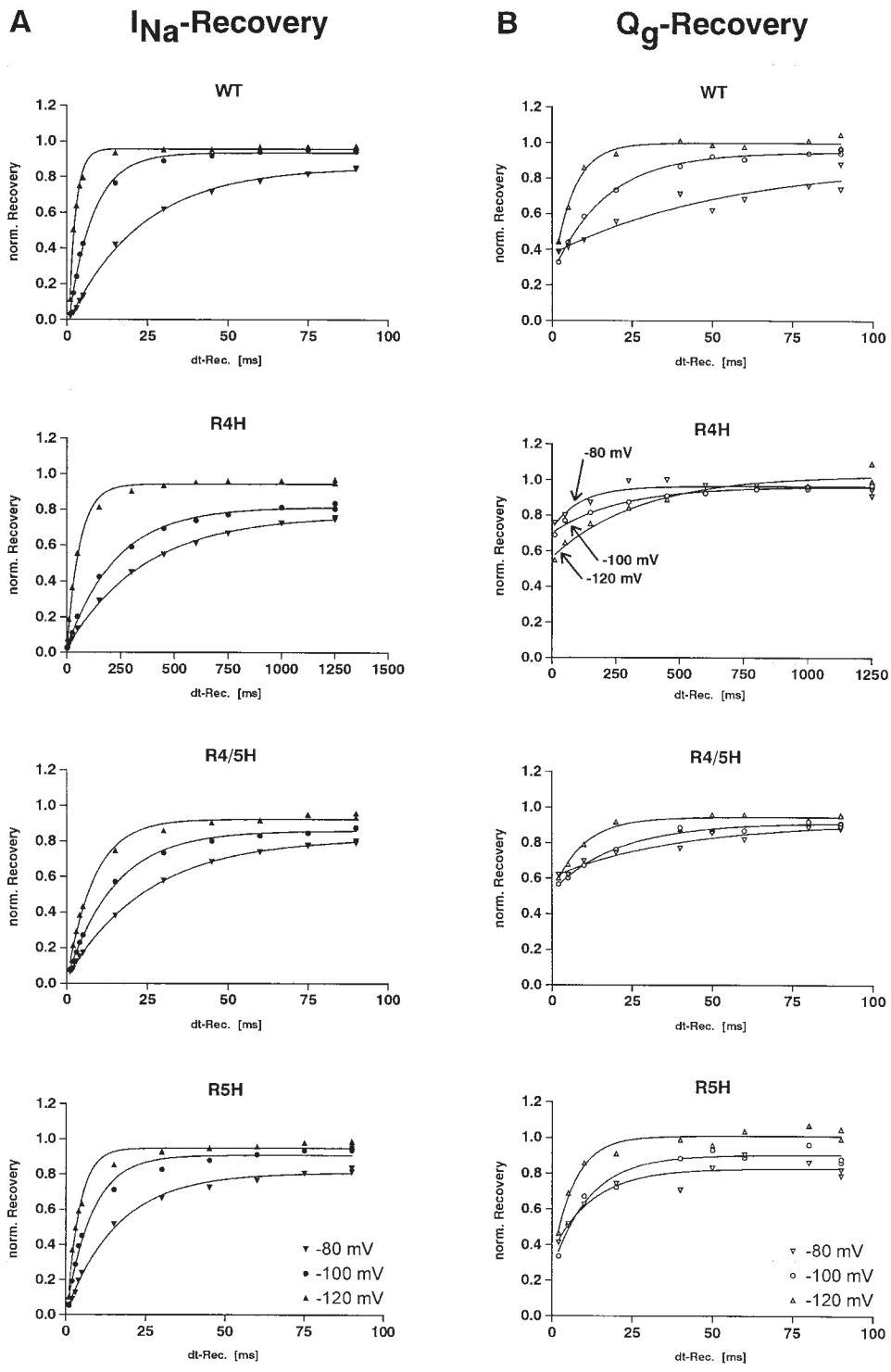

Figure 6. Comparison of the recovery of ionic current and gating charge of WT and mutant sodium channels at different potentials. Sodium current recovery (left panel) and gating charge recovery (right panel) at recovery potentials of −80, −100, and −120 mV in WT-, R4H-, R4/5H-, and R5H-sodium channels. The data of each subdiagram were recorded from different oocytes and normalized as described in Fig. 5. Notice the different starting points of gating current recovery in R4H that strictly depend on the effective recovery potential (indicated by arrows). Corresponding sodium current (I_{Na}) and gating charge (Q_g) recovery time constants obtained from single exponential fits are as follows (I_{Na}/Q_g in ms): WT, 22.8/54.9 (−80 mV), 7.6/16.7 (−100 mV), 2.1/6.4 (−120 mV); R4H, 359/113 (−80 mV), 228/269 (−100 mV), 59.7/349 (−120 mV); R4/5H, 25.4/39.7 (−80 mV), 14.9/20.6 (−100 mV), 8.4/9.5 (−120 mV); R5H, 16.3/12.6 (−80 mV), 8.0/11.6 (−100 mV), 3.8/6.9 (−120 mV).

the sodium reversal potential (E_{Na}). Subsequently, we recorded the ionic current recovery at a potential slightly below E_{Na}, yielding relatively small sodium currents minimally distorted by R_s errors. The partial reduction of sodium currents with submaximal concentrations of TTX was avoided due to the phenomenon of use-dependent block (Patton and Goldin, 1991). The comparison of the sequences of ionic and gating current traces in Fig. 7 C indicates that the corresponding recovery time courses should be similar, and indeed the resulting recovery time constants are almost identical (Fig. 7 A, triangles). Thus, the observed discrepancy between ionic and gating current recovery time constants within a single phenotype may be at least par-

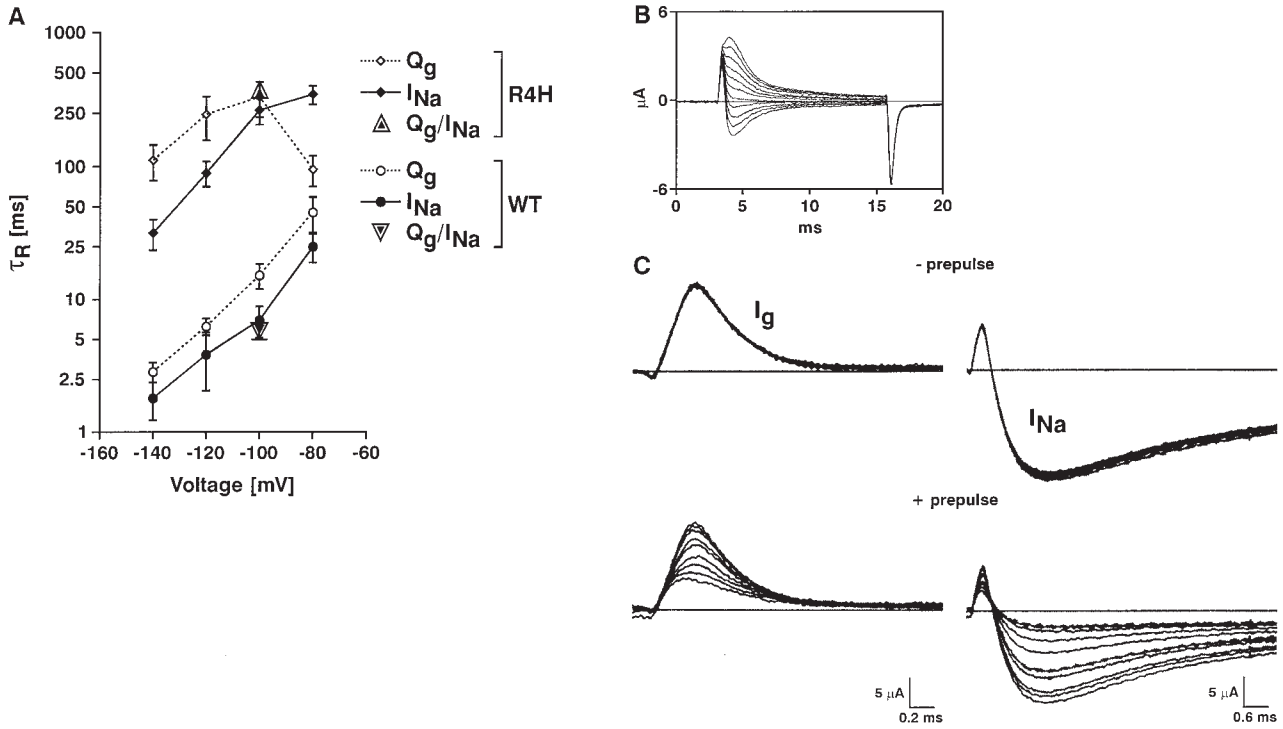

Figure 7. Correlation of the recovery of ionic current and gating charge of WT and R4H at different potentials. (A) Semilogarithmic plot of ionic current (filled symbols) and gating charge (open symbols) recoveries obtained from different oocytes are superimposed for potentials of −140, −120, −100, and −80 mV. Values are mean ± SD of $n > 3$ cells. Superimposed triangles represent congruent data of ionic current (small, filled triangle) and gating charge recovery (large, open triangle) recorded sequentially in a single oocyte at −100 mV. (B) Simultaneous recording of ionic and gating currents around sodium reversal potential (E_{Na}). Test pulses elicited from +5 to +15 mV in steps of 1 mV, holding potential −100 mV. Extracellular sodium concentration was reduced to 8.8 mM by choline replacement in Modified Barth's Solution. Ionic currents change polarity when crossing E_{Na}, whereas gating currents follow the direction of the electric field. (C) Recordings of gating current and ionic current recovery at sodium reversal potential (E_{Na}) obtained from a single oocyte, T = 8°C. Pulse-protocol: a 20 ms prepulse to 40 mV was followed by a recovery period of variable duration (1–60 ms) at −100 mV and a test pulse to −20 (ionic current) or 34 mV (E_{Na}; gating current), test pulse duration 13 ms, holding potential −100 mV.

tially caused by performing the recovery experiments in separate oocytes and at different times of expression.

The most important conclusions from these experiments are that a point mutation in the central part of S4D4 (R4H) is able to slow down both the release of the inactivation loop and the return of the immobilized voltage sensors similarly in a drastic and voltage-dependent manner, suggesting that these two processes are structurally interconnected; and that the mutation R4H considerably reduces the degree of immobilization in both the single and double mutant, most probably by stabilizing the inactivated state.

discussion

The currently available data suggest that only the outermost arginines (R1–R3) represent the voltage-sensing part of S4D4 (Yang et al., 1996), whereas the function of the similarly conserved arginines of the central and innermost part of S4D4 remains uncertain (Abbruzzese et al., 1998). On the other hand, the fact that S4D4 mutations primarily affect the inactivation properties of the sodium channel (Chahine et al., 1994; Chen et al., 1996; Kontis and Goldin, 1997) suggests that there might be some structural coupling between this voltage sensor and the inactivation gate. Therefore, the approach of this study was to modify the S4 voltage sensor in domain 4 by mutation of the central arginines to histidines and in this way possibly affect the time course of fast inactivation. The selected mutations should result in a partial charge neutralization and, due to the bulky histidine side chain, probably to an altered local structure within the central part of S4D4.

According to the present understanding (Fig. 8 A), the S4–S5 linker in domain 4 represents part of the putative receptor that binds the docking region of the intracellular loop connecting domains 3 and 4 (Tang et al., 1996; Mitrovic et al., 1996; Filatov et al., 1998; McPhee et al., 1998). This loop contains a highly conserved triplet of three consecutive amino acids (IFM: isoleucine-phenylalanine-methionine) and is regarded as the physical inactivation gate (Vassilev et al., 1988;

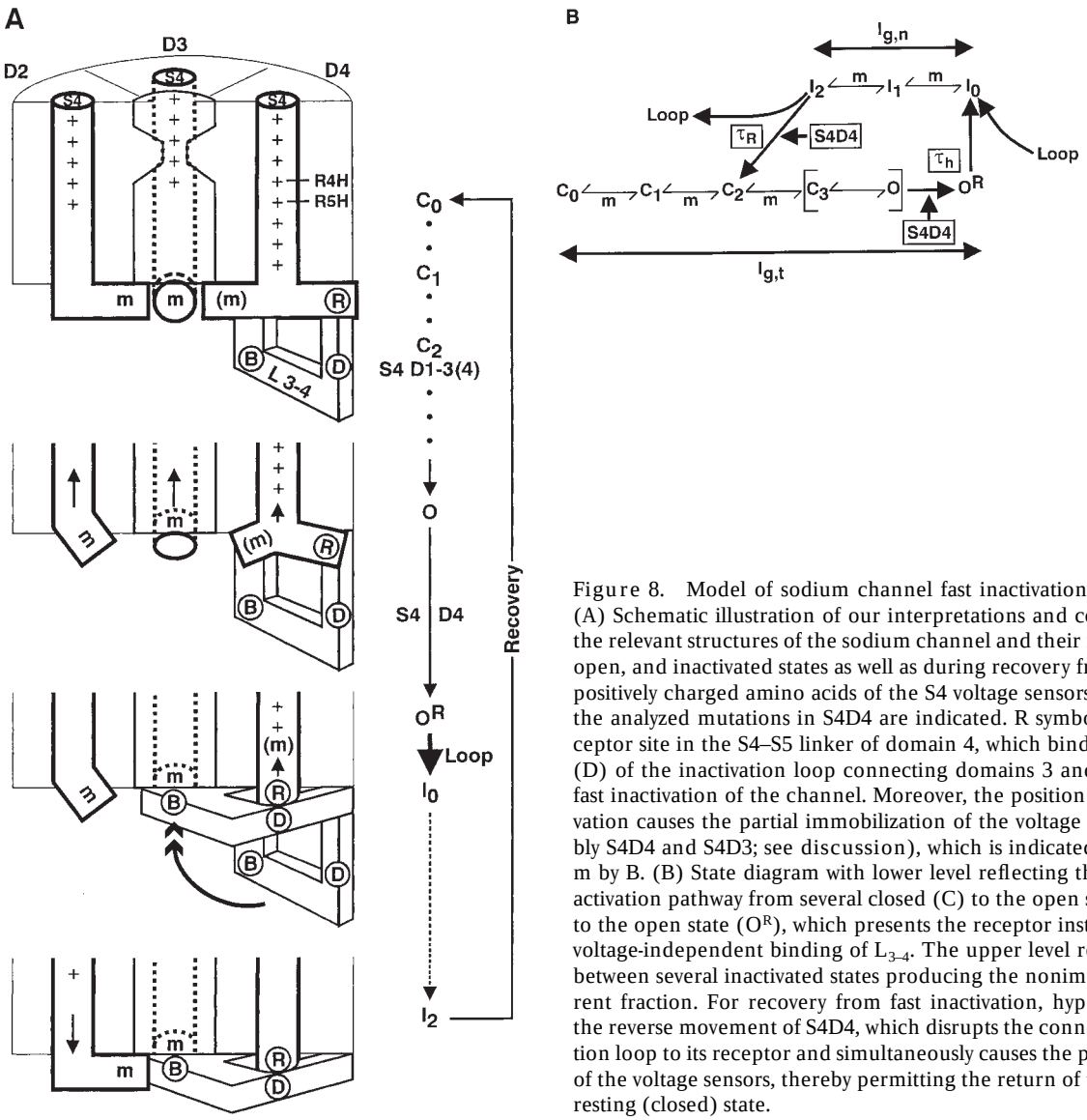

Figure 8. Model of sodium channel fast inactivation controlled by S4D4. (A) Schematic illustration of our interpretations and conclusions displaying the relevant structures of the sodium channel and their movements at closed, open, and inactivated states as well as during recovery from inactivation. The positively charged amino acids of the S4 voltage sensors in domains 2–4 and the analyzed mutations in S4D4 are indicated. R symbolizes the putative receptor site in the S4–S5 linker of domain 4, which binds the docking region (D) of the inactivation loop connecting domains 3 and 4 (L_{3-4}), leading to fast inactivation of the channel. Moreover, the position of L_{3-4} during inactivation causes the partial immobilization of the voltage sensors (most probably S4D4 and S4D3; see discussion), which is indicated here as blockade of m by B. (B) State diagram with lower level reflecting the voltage-dependent activation pathway from several closed (C) to the open state (O) and further to the open state (O^R), which presents the receptor instantly followed by the voltage-independent binding of L_{3-4}. The upper level reflects the transitions between several inactivated states producing the nonimmobilized gating current fraction. For recovery from fast inactivation, hyperpolarization causes the reverse movement of S4D4, which disrupts the connection of the inactivation loop to its receptor and simultaneously causes the partial immobilization of the voltage sensors, thereby permitting the return of the channels into the resting (closed) state.

Stühmer et al., 1989; West et al., 1992; Eaholtz et al., 1994). In addition, gating current studies at the squid axon showed the partial immobilization of gating current and gave rise to the idea of the "foot in the door" effect, i.e., an obstacle in the restoration of some gating structures during recovery from inactivation (Armstrong and Bezanilla, 1977). Our study is to contribute to the understanding of how these different structures may be functionally connected and in particular how the voltage sensor S4D4 is coupled to fast inactivation and gating charge immobilization. Besides fast inactivation, which proceeds over milliseconds during brief depolarizations (<100 ms), sodium channels can inactivate over a much longer time scale when depolarized for seconds or minutes, a phenomenon called slow inactivation. Previously, little has been known about the structural basis of slow inactivation, but recent experimental data suggest that S4D4 plays an important role also in slow inactivation (Abbruzzese et al., 1998; Mitrovic and Horn, 1999). However, these studies have not analyzed the electrophysiologically silent transitions between different inactivated states because gating current measurements were not performed. In addition, Vedantham and Cannon (1998) have demonstrated that in voltage-gated sodium channels slow inactivation does not affect the movement of the fast inactivation gate. Because our approach was to correlate the movements of the S4D4 voltage sensor and the fast inactivation gate using ionic and gating current recordings, we performed our experiments under conditions that minimize the possible effects of slow inactivation.

We found that the mutation of neighbored arginines

in the central part of S4D4 either markedly increases the inactivation time constant (in R5H; Fig. 2) or drastically increases the recovery time constant (in R4H; Figs. 1 D and 7 A). Therefore, the two mutants display opposite preferences for the open state and the inactivated state, respectively (Fig. 1 C). On the other hand, the voltage dependencies are hardly changed in either the single or the double mutant (Figs. 1 D, 2, and 7 A). This supports the results of Yang et al. (1996) that only the outermost arginines (R1, R2, R3) sense the transmembranal electric field.

The actual inactivation process is commonly regarded as a binding of L_{3-4} to a receptor site that occurs without voltage dependence in the cytoplasm. With respect to our data we propose that the binding of the inactivation loop to a receptor site at the intracellular mouth of the channel depends on the movement of S4D4; the receptor must first be accessible and then immediately a strong binding of L_{3-4} occurs. On one hand, the presentation of the receptor is delayed in R5H, which results in a slowed inactivation, and on the other, the release of L_{3-4} from the receptor is delayed in R4H, which extends recovery time from inactivation. In the state diagram (Fig. 8 B), this is interpreted as a voltage-dependent conformational change to reach O^R, the open state that presents the receptor instantly followed by the voltage-independent binding of L_{3-4} leading to the closure of the pore. For recovery from fast inactivation, hyperpolarization should cause the reverse movement of S4D4 and thereby disrupts the binding of the loop to its receptor. Therefore, any mutation that impedes the mobility of S4D4 should have a strong impact on either the inactivation time constant or the recovery time constant.

The macroscopic detectable degree of charge immobilization also reflects the distribution of the channels between the level of the inactivated states ($I_{g,n}$ level in Fig. 8 B) and the level of the C/O states ($I_{g,t}$ level in Fig. 8 B). This means that the actual ratio of channels producing the total gating current fraction ($I_{g,t}$) and channels that produce the nonimmobilized gating current fraction ($I_{g,n}$) determines the apparent immobilization properties due to an inactivating prepulse. Accordingly, the maximum degree of charge immobilization is obtained when all channels move from the leftmost closed state (C_0) to the rightmost inactivated state (I_0) during the test pulse and will switch between the I states during the short recovery period after an inactivating prepulse (ratio of $I_{g,n}/I_{g,t}$ is minimal). However, if the inactivated states are already occupied at the holding potential by a fraction of channels, this fraction will always produce $I_{g,n}$ even without inactivating prepulse. Hence, the fraction of channels producing $I_{g,t}$ is smaller, leading to a reduced degree of apparent charge immobilization. As can be clearly deduced from Fig. 6, the degree of immobilization in R4H depends on the effective membrane potential. This means that for more hyperpolarizing potentials (−120 mV) the number of channels passing along the $I_{g,t}$ level is markedly increased whereas, for more depolarizing potentials (−80 mV) the majority of the channels stay on the $I_{g,n}$ level. This is consistent with our observation that at a holding potential of −80 mV the ionic current of R4H is profoundly decreased (not recognizable in Fig. 6 A because data were normalized). The slightly reduced degree of immobilization in R5H channels compared with WT (Table I) is due to the fact that fast inactivation and with it the immobilization process is slowed and incomplete (indicated by the distinct plateau current of R5H in Fig. 2 A). Consequently, there are less channels at the $I_{g,n}$ level and more channels moving in both directions at the $I_{g,t}$ level even after an inactivating prepulse. Finally, the double mutant represents a combination of the R4H and R5H phenotypes showing both slowed and incomplete immobilization and likewise a moderately delayed recovery from immobilization that lead to a degree of immobilization similar to R4H. An additional explanation for the reduction of charge immobilization in R4H and R4/5H may be that the (partial) neutralization of the positively charged arginine R4 leads to a small reduction of $I_{g,t}$. In contrast, for R5H this would be less the case, because according to Yang et al. (1996) R5 hardly senses the membrane voltage.

Regarding the theoretical capacity of S4D4 to contribute to the total gating charge, the degree of immobilization in WT channels implies that not only S4D4 is immobilized during inactivation but that S4 segments of other domains are at least partially involved. Our data do not permit a conclusion as to whether S4D4 and one additional S4 segment of another domain are completely blocked, whereas the two remaining S4 segments are free to move, or whether the return of several S4 segments is partially limited during inactivation. Meanwhile, Cha et al. (1999) have demonstrated that the voltage sensors in domains 3 and 4 but not 1 and 2 are immobilized during sodium channel fast inactivation using site-directed fluorescent labeling and gating current measurements. These results are consistent with our data, but in the same study it was supposed that the return of the immobilized charge is rate limited by S4D3. However, this conclusion is not fully convincing to us because Cha et al. (1999) have also observed that only the domain 4 mutant showed substantial kinetic differences from the WT channel. Moreover, they found that the signal to noise in the fluorescence traces is poor in domain 4. Therefore, the comparison of S4 mutants of all four domains that display partly different effects on channel kinetics might be problematic. In contrast, our study was limited to S4D4, but the

data clearly indicate that S4D4 is at least one of the voltage sensors that is immobilized. Moreover, the results support the hypothesis that the movement of S4D4 directly controls the interaction of the inactivation loop with its putative receptor site and consequently the immobilization of further S4 voltage sensors, most likely S4D3 (Cha et al., 1999). On the other hand, the fast return of the S4 voltage sensors of domains 1 and 2 producing the nonimmobilized gating current fraction ($I_{g,n}$) may be related to a fast closure of part of the activation machinery preventing channel reopening during recovery (Armstrong, 1981; Cha et al., 1999).

According to our molecular model (Fig. 8), the open state that presents the receptor (O^R) is reached under control of S4D4. The nature of the preceding states (Fig. 8 B, shown in brackets) will be discussed now: if O^R were preceded by a closed state, S4D4 would simultaneously participate in activation and inactivation. Hence, the S4D4 mutations should slow the inactivation and activation kinetics in parallel, which is not the case as far we can judge (see Fig. 2 B), even taking into account some limitations of the clamp speed. Therefore, an activation step from a closed into an open state ($C \rightarrow O$) that is not affected by the S4D4 mutations appears necessary. Accordingly, the channel stays open during a voltage-dependent phase ($O \rightarrow O^R$), which is terminated by the voltage-independent attachment of the inactivation gate L_{3-4} to the receptor. Moreover, this concept implicates that the mutation R5H impedes the entry into the O^R state and not the transition into the I state. This means that the mean open time of R5H should be prolonged and voltage dependent both in WT and mutant channels, and that the R5H channels were not absorbed into the I state since the $O^R \rightarrow I$ rates should be undisturbed, which is indicated by the macroscopic plateau currents of this mutant (see Fig. 2 A).

However, the analysis of our mutants on the single channel level has to be studied further. Interestingly, McPhee et al. (1998) have shown that a mutation adjacent to R5H (L1639A) similarly displays an increase of τ_h and furthermore has a prolonged single channel mean open time. In contrast, the mutations in the proposed receptor region, L1660A and N1662A show a burst of short openings as would be expected when the attachment of L_{3-4} to the receptor in S4–S5D4 is changed. Finally, the putative receptor region identified by McPhee et al. (1998) is only $\sim$10 amino acids distant from the inner end of the voltage sensor. This may support our hypothesis that the receptor site is exposed under control of S4D4.

The $C \rightarrow O$ transition either could be caused exclusively by the movement of the S4 voltage sensors of domain 1–3, or by S4D4 participating in activation during a first step and initiating inactivation during a second step (illustrated in Fig. 8). There could also be another two-step process, where the first step of S4D4 just produces some delay before the second step starts inactivation by presentation of the receptor. Although these alternative pathways remain to be cleared in further studies, the main conclusion of this study is that sodium channel fast inactivation is strongly coupled to the mobility of the S4D4 voltage sensor. Then a gating current component should exist that parallels the movement of the inactivation gate. This component is expected to be slow and small in amplitude, as discussed in a previous study, where evidence for such a component had been obtained in high resolution recordings at the squid giant axon (Greeff and Forster, 1991).

The observed strong but antagonistic effects of R4H and R5H on the inactivation properties of the sodium channel as well as the phenotype of the double mutant R4/5H support the idea that the central section of S4D4 plays an important role in controlling the movement of the voltage sensor in either direction. Therefore, we propose that the residues R4 and R5 are localized at a critical position concerning the interaction of S4D4 with surrounding channel structures.

Yang et al. (1996) have studied the accessibility of S4D4 residues from the intracellular or extracellular side of the membrane by cysteine scanning mutagenesis in human skeletal muscle sodium channels. They found that R4 and R5 are exclusively accessible from the intracellular side both at depolarizing and hyperpolarizing potentials, whereas R3 and R2 alter their accessibility in response to changes in the membrane electric field. Consequently, the outermost residues of S4D4 should play a crucial role in the voltage dependence of channel gating. The analysis of charge neutralizing mutations concerning these residues in sodium channels of human skeletal muscle (Chahine et al., 1994) and human heart (Chen et al., 1996) clearly support this hypothesis.

Accordingly, it is conceivable that R4 and R5 could be critical determinants for the voltage-driven shift of R2 and R3 involved in the structural interactions that are necessary for this movement. With respect to the observed antagonism, we propose that negative counter charges affect the movement of the positively charged S4D4 residues inside the hydrophobic protein core. For *Shaker* potassium channels it was demonstrated that there are electrostatic interactions between the positively charged residues of the central to innermost section in S4 and the negatively charged residues in S2 (Papazian et al., 1995). Histidine has, depending on the local protein environment, a pK of 5.6–7.0 and therefore should carry less positive charge than arginine at physiological pH (Sancho et al., 1992). However, this means that the mutation of arginine to histidine most likely is not completely charge neutralizing. It is obvious that the side chains of histidine and argi-

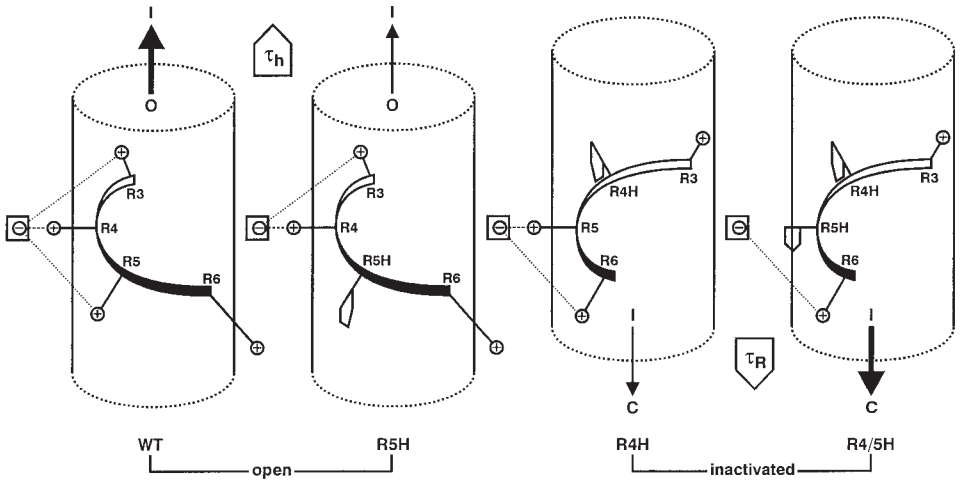

Figure 9. Scheme of possible interactions of the central arginines of S4D4 with a putative counter-charge that could explain the different inactivation behavior of the mutants. Illustrated is the central section of S4D4 containing the highly conserved central arginines R3–R6; the hypothetical negative counter-charge is indicated. WT and R5H are shown in the open state and R4H and R4/5H are shown in the inactivated state. Compared with WT, the O → I transition is considerably slowed in R5H (indicated by a thin arrow) and moderately slowed in R4H (not illustrated). This is due to the electrostatic asymmetry resulting from the interaction of the negative counter-charge with the neighbored arginines and histidines in the single mutants. On the other hand, the $I_2 \rightarrow C_2$ transition (recovery from inactivation) is for the same reason drastically slowed in R4H (indicated by a thin arrow) and hardly affected in R5H (not illustrated). In contrast, WT and R4/5H display more symmetrical electrostatics, but due to the considerably altered structure in the double mutant, the mobility of S4D4 is slowed in both directions.

nine have a distinctly different molecular structure. This gives rise to the assumption that the mutations R4H, R4/5H, and R5H could markedly change the local structure and at least partially change the charge distribution (Fig. 9).

Thus, if either R4 or R5 is replaced by a histidine this leads to a local electrostatic asymmetry and a putative negative countercharge stabilizes either R4(+)-H5 in the open state or H4-R5(+) in the inactivated state (Fig. 9). In contrast, in WT the electrostatics are more symmetrical, which allows S4 to move readily in both directions. The electrostatic asymmetry is less pronounced in R4/5H than in the single mutants, leading only to a moderate increase of the inactivation and recovery time constants when compared with WT. The results of Abbruzzese et al. (1998), which have mutated the corresponding arginines to glutamines in rSkM sodium channels, fit our antagonism model even better. They found that R4Q shows a decreased inactivation time constant and up to ten times slower recovery than WT, whereas R5Q displays an increased inactivation time constant and an accelerated recovery from fast inactivation.

In general, it is rather difficult to compare different mutations without having precise information about the local secondary and tertiary structure of the protein. However, it is possible that the exchange of arginine by the bulky histidine in our study generally slows the mobility of S4D4 in the mutant channels in both directions ($O \rightarrow O^R$ and $I_2 \rightarrow C_2$; see Fig. 8 B), which is particularly apparent in the double mutant. This effect could cover the clear antagonism of the charge neutralizing mutations R4Q and R5Q observed by Abbruzzese et al. (1998).

Consistent with this idea is the hypothesis of Ji et al. (1996), who have suggested that segment 3 (S3) in domain 4 is important for the control of the movement of S4D4 by maintaining an optimal local environment where hydropathy is an substantial factor.

Finally, another obvious explanation for the different results could be the coexpression of the β1 subunit by Abbruzzese et al. (1998). We cannot exclude that the absence of β1 coexpression generally slows the kinetics of WT and mutant channels in our study regardless of our observation that the β1 effect is markedly decreased at very high expression levels. Unfortunately, we were not able to analyze the data of Abbruzzese et al. (1998) in detail from the short abstract information.

In our view, the ball and chain hypothesis would be well compatible with voltage-dependent inactivation if one assumes an interaction of the inactivation loop with the cytoplasmic extension of the S4D4 voltage sensor, i.e., the S4–S5 linker. Considering the presently available data, it seems very likely that the actual receptor for the inactivation gate resides in the vicinity of S4D4.

We thank Dr. Alan L. Goldin for providing the cDNA of the WT rBIIA sodium channel (pVA2580) and the high expression vector (pBSTA), as well as for valuable advice and discussions; we also thank Christian Gasser for his graphical assistance as well as Wolfgang Kathe and Dr. Kevin Martin for helpful discussion and comments on the manuscript.

The work was supported by the Swiss National Science Foundation (grant 31-37987.93) and the Hartmann-Müller-Stiftung.

Submitted: 18 March 1999 Revised: 17 May 1999 Accepted: 27 May 1999

references

Abbruzzese, J.L., E. Fujimoto, and P.C. Ruben. 1998. Differential effects on fast inactivation of domain IV S4 charge neutralizations. *Biophys. J.* 74:A401. (Abstr.)

Aggarwal, S.K., and R. MacKinnon. 1996. Contribution of the S4 segment to gating charge in the *Shaker* K^+ channel. *Neuron*. 16: 1169–1177.

Aldrich, R.W., D.P. Corey, and C.F. Stevens. 1983. A reinterpretation of mammalian sodium channel gating based on single channel recording. *Nature*. 306:436–441.

Armstrong, C.M. 1981. Sodium channels and gating currents. *Physiol. Rev.* 61:644–683.

Armstrong, C.M., and F. Bezanilla. 1977. Inactivation of the sodium channel. II. Gating current experiments. *J. Gen. Physiol*. 70: 567–590.

Armstrong, C.M., and B. Hille. 1998. Voltage-gated ion channels and electrical excitability. *Neuron*. 20:371–380.

Bezanilla, F., E. Perozo, and E. Stefani. 1994. Gating of *Shaker* K^+ channels. II. The components of gating currents and a model of channel activation. *Biophys. J.* 66:1011–1021.

Catterall, W.A. 1986. Molecular properties of voltage-sensitive sodium channels. *Ann. Rev. Biochem*. 55:953–985.

Cha, A., P.C. Ruben, A.L. George, Jr., E. Fujimoto, and F. Bezanilla. 1999. Voltage sensors in domains III and IV, but not I and II are immobilized by Na^+ channel fast inactivation. *Neuron*. 22:73–87.

Chahine, M., A.L. George, Jr., M. Zhou, S. Ji, W. Sun, R.L. Barchi, and R. Horn. 1994. Sodium channel mutations in paramyotonia congenita uncouple inactivation from activation. *Neuron*. 12: 281–294.

Chen, L.-Q., V. Santarelli, R. Horn, and R.G. Kallen. 1996. A unique role for the S4 segment of domain 4 in the inactivation of sodium channels. *J. Gen. Physiol*. 108:549–556.

Conti, F., and W. Stühmer. 1989. Quantal charge redistributions accompanying the structural transitions of sodium channels. *Eur. Biophys. J.* 17:53–59.

Durell, S.R., and H.R. Guy. 1992. Atomic scale structure and functional models of voltage-gated potassium channels. *Biophys. J.* 62: 238–247.

Eaholtz, G., T. Scheuer, and W.A. Catterall. 1994. Restoration of inactivation and block of open sodium channels by an inactivation gate peptide. *Neuron*. 12:1041–1048.

Filatov, G.N., T.P. Nguyen, S.D. Kraner, and R.L. Barchi. 1998. Inactivation and secondary structure in the D4/S4-5 region of the SkM1 sodium channel. *J. Gen. Physiol*. 111:703–715.

Greeff, N.G. 1986. Fractionation of the asymmetry current and its relation to sodium channel gating in squid axon. *In* Ion Channels in Neural Membranes. J.M. Ritchie, R.D. Keynes, and L. Bolis, editors. R. Alan Liss Inc., New York, NY. 53–69.

Greeff, N.G., and I.C. Forster. 1991. The quantal gating charge of sodium channel inactivation. *Eur. Biophys. J.* 20:165–176.

Greeff, N.G., and R. Polder. 1998. Optimization of a two-electrode voltage clamp for recording of sodium ionic and gating currents from *Xenopus* oocytes. *Biophys. J.* 74:A402. (Abstr.)

Greeff, N.G., F.J.P. Kühn, and W. Kathe. 1998. Gating current in rat brain IIA sodium channels: changes in ratio between measured gating and corresponding ionic currents. *Biophys. J.* 74:A402. (Abstr.)

Hodgkin, A.L., and A.F. Huxley. 1952. A quantitative description of membrane current and its application to conduction and excitation in nerve. *J. Physiol*. 117:500–544.

Ji, S., A.L. George, Jr., R. Horn, and R.L. Barchi. 1996. Paramyotonia congenita mutations reveal different roles for segments S3 and S4 of domain D4 in hSkM1 sodium channel gating. *J. Gen. Physiol*. 107:183–194.

Kontis, K.J., and A. Goldin. 1997. Sodium channel inactivation is altered by substitution of voltage sensor positive charges. *J. Gen. Physiol*. 110:403–413.

Kontis, K.J., A. Rounaghi, and A. Goldin. 1997. Sodium channel activation gating is affected by substitutions of voltage sensor positive charges in all four domains. *J. Gen. Physiol*. 110:391–401.

Krafte, D.S., A.L. Goldin, V.J. Auld, R.J. Dunn, N. Davidson, and H.A. Lester. 1990. Inactivation of cloned Na channels in *Xenopus* oocytes. *J. Gen. Physiol*. 96:689–706.

McPhee, J.C., T.S. Ragsdale, T. Scheuer, and W.A. Catterall. 1998. A critical role for the S4-S5 intracellular loop in domain IV of the sodium channel α-subunit in fast inactivation. *J. Biol. Chem*. 273: 1121–1129.

Mitrovic, N., and R. Horn. 1999. Role of the D4/S4 segment in slow inactivation of sodium channels. *Biophys. J.*, 76:A194. (Abstr.)

Mitrovic, N., H. Lerche, R. Heine, R. Fleischhauer, U. Pika-Hartlaub, U. Hartlaub, A.L. George, and F. Lehmann-Horn. 1996. Role in fast inactivation of conserved amino acids in the IV/S4-S5 loop of the human muscle Na^+ channel. *Neurosci. Lett.* 214:9–12.

Moran, O., and F. Conti. 1990. Sodium ionic and gating currents in mammalian cells. *Eur. Biophys. J.* 18:25–32.

Noda, M., T. Ikeda, H. Suzuki, H. Takeshima, H. Takahashi, M. Kuno, and S. Numa. 1986. Expression of functional sodium channels from cloned cDNA. *Nature*. 322:826–828.

Papazian, D.M., and F. Bezanilla. 1997. How does an ion channel sense voltage? *News in Physiological Sciences*. 12:203–210.

Papazian, D.M., L.C. Timpe, Y.N. Jan, and L.Y. Jan. 1991. Alteration of voltage-dependence of *Shaker* potassium channel by mutations in the S4 sequence. *Nature*. 349:305–310.

Papazian, D.M., X.M. Shao, S.-A. Seoh, A.F. Mock, Y. Huang, and D.H. Wainstock. 1995. Electrostatic interactions of S4 voltage sensor in *Shaker* K^+ channel. *Neuron*. 14:1293–1301.

Patton, D.E., and A.L. Goldin. 1991. A voltage-dependent gating transition induces use-dependent block by tetrodotoxin of rat IIA sodium channels expressed in *Xenopus* oocytes. *Neuron*. 7:637–647.

Patton, D.E., L.L. Isom, W.A. Catterall, and A.L. Goldin. 1994. The adult rat brain β_1 subunit modifies activation and inactivation gating of multiple sodium channel α subunits. *J. Biol. Chem*. 269: 17649–17655.

Ptàcek, L.J., A.L. George, Jr., R.L. Barchi, R.C. Griggs, J.E. Riggs, M. Robertson, and M.F. Leppert. 1992. Mutations in an S4 segment of the adult skeletal muscle cause paramyotonia congenita. *Neuron*. 8:891–897.

Roux, M.J., R. Olcese, L. Toro, F. Bezanilla, and E. Stefani, 1998. Fast inactivation in *Shaker* K^+ channels. Properties of ionic and gating currents. *J. Gen. Physiol*. 111:625–638.

Ruben, P.C., A. Fleig, D. Featherstone, J.G. Starkus, and M.D. Rayner. 1997. Effects of clamp rise-time on rat brain IIA sodium channels in *Xenopus* oocytes. *J. Neurosci. Meth*ods. 73:113–122.

Sancho, J., L. Serrano, and A.R. Fersht. 1992. Histidine residues at the N- and C-termini of α-helices: perturbed pK_as and protein stability. *Biochemistry.* 31:2253–2258.

Schreibmayer, W., H.A. Lester, and N. Dascal. 1994. Voltage clamping of *Xenopus* laevis oocytes utilizing agarose-cushion electrodes. *Pflügers Arch*. 426:453–458.

Seoh, S.-A., D. Sigg, D.M. Papazian, and F. Bezanilla. 1996. Voltage-sensing residues in S2 and S4 segments of the *Shaker* K^+ channel. *Neuron*. 16:1159–1167.

Shih, T.M., R.D. Smith, L. Toro, and A.L. Goldin. 1998. High-level expression and detection of ion channels in *Xenopus* oocytes. *Methods Enzymol*. 293:529–556.

Sigworth, F.J. 1993. Voltage gating of ion channels. *Quart. Rev. Biophys*. 27:1–40.

Sheets, M.F., and D.A. Hanck. 1995. Voltage-dependent open-state inactivation of cardiac sodium channels: gating current studies with Anthopleurin-A toxin. *J. Gen. Physiol.* 106:617–640.

Stefani, E., L. Toro, E. Perozo, and F. Bezanilla. 1994. Gating of *Shaker* K^+ channels. I. Ionic and gating currents. *Biophys. J.* 66: 996–1010.

Stühmer, W., F. Conti, H. Suzuki, X. Wang, M. Noda, N. Yahagi, H. Kubo, and S. Numa. 1989. Structural parts involved in activation and inactivation of the sodium channel. *Nature.* 339:597–603.

Tang, L.H., R.G. Kallen, and R. Horn. 1996. Role of an S4-S5 linker in sodium channel inactivation probed by mutagenesis and a peptide blocker. *J. Gen. Physiol.* 108:89–104.

Vassilev, P.M., T. Scheuer, and W.A. Catterall. 1988. Identification of an intracellular peptide segment involved in sodium channel inactivation. *Science.* 241:1658–1661.

Vedantham, V., and S.C. Cannon. 1998. Slow inactivation does not affect movement of the fast inactivation gate in voltage-gated Na^+ channels. *J. Gen. Physiol.* 111:83–93.

West, J.W., D.E. Patton, T. Scheuer, Y. Wang, A.L. Goldin, and W.A. Catterall. 1992. A cluster of hydrophobic amino acid residues required for fast sodium channel inactivation. *Proc. Natl. Acad. Sci. USA.* 89:10910–10914.

Yang, N., and R. Horn. 1995. Evidence for voltage dependent S4 movements in sodium channels. *Neuron.* 15:213–218.

Yang, N.B., A.L. George, and R. Horn. 1996. Molecular basis of charge movement in voltage-gated sodium channels. *Neuron.* 16:113–122.